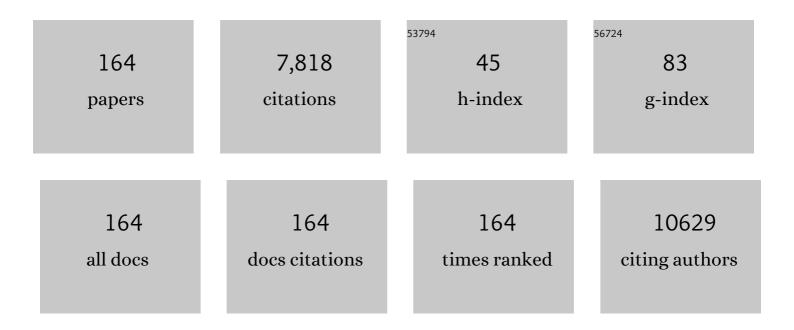
## Anmin Nie

List of Publications by Year in descending order

Source: https://exaly.com/author-pdf/2480977/publications.pdf Version: 2024-02-01



#	Article	IF	CITATIONS
1	Discovery of carbon-based strongest and hardest amorphous material. National Science Review, 2022, 9, nwab140.	9.5	49
2	Controllable growth of multilayered XSe <sub>2</sub> (X = W and Mo) for nonlinear optical and optoelectronic applications. 2D Materials, 2022, 9, 015012.	4.4	2
3	Ultrasensitive biochemical sensors based on controllably grown films of high-density edge-rich multilayer WS2 islands. Sensors and Actuators B: Chemical, 2022, 353, 131081.	7.8	5
4	Extreme dislocation-mediated plasticity of yttria-stabilized zirconia. Materials Today Physics, 2022, 22, 100588.	6.0	1
5	Broadband light absorption and photoresponse enhancement in monolayer WSe2 crystal coupled to Sb2O3 microresonators. Nano Research, 2022, 15, 4653-4660.	10.4	5
6	Scalable Van der Waals Encapsulation by Inorganic Molecular Crystals. Advanced Materials, 2022, 34, e2106041.	21.0	18
7	Enabling Anionic Redox Stability of P2â€Na <sub>5/6</sub> Li <sub>1/4</sub> Mn <sub>3/4</sub> O <sub>2</sub> by Mg Substitution. Advanced Materials, 2022, 34, e2105404.	21.0	46
8	Scalable Van der Waals Encapsulation by Inorganic Molecular Crystals (Adv. Mater. 7/2022). Advanced Materials, 2022, 34, .	21.0	0
9	Well-controlled Core-shell structures based on Fe3O4 nanospheres coated by polyaniline for highly efficient microwave absorption. Applied Surface Science, 2022, 591, 153176.	6.1	35
10	Siliconâ€Phosphorusâ€Nanosheetsâ€Integrated 3Dâ€Printable Hydrogel as a Bioactive and Biodegradable Scaffold for Vascularized Bone Regeneration. Advanced Healthcare Materials, 2022, 11, e2101911.	7.6	23
11	Structural Insights into the Lithium Ion Storage Behaviors of Niobium Tungsten Double Oxides. Chemistry of Materials, 2022, 34, 388-398.	6.7	21
12	Flexible Aramid Nanofiber/Bacterial Cellulose/Graphene Papers with Nickel Nanoparticles for Enhanced Electromagnetic Interference Shielding and Joule Heating Performance. ACS Applied Nano Materials, 2022, 5, 5589-5598.	5.0	14
13	Multifunctional Bacterial Cellulose Nanofibers/Polypyrrole (PPy) Composite Films for Joule Heating and Electromagnetic Interference Shielding. ACS Applied Electronic Materials, 2022, 4, 2552-2560.	4.3	14
14	Engineering a Local Free Water Enriched Microenvironment for Surpassing Platinum Hydrogen Evolution Activity. Angewandte Chemie, 2022, 134, .	2.0	8
15	Achieving Stable Cycling of LiCoO <sub>2</sub> at 4.6 V by Multilayer Surface Modification. Advanced Functional Materials, 2021, 31, 2001974.	14.9	77
16	Room-temperature plasticity in diamond. Science China Technological Sciences, 2021, 64, 32-36.	4.0	9
17	High-performance flexible all-solid-state micro-supercapacitors based on two-dimensional InSe nanosheets. Journal of Power Sources, 2021, 482, 228987.	7.8	10
18	Broadband photodetector of high quality Sb2S3 nanowire grown by chemical vapor deposition. Journal of Materials Science and Technology, 2021, 75, 14-20.	10.7	34

#	Article	IF	CITATIONS
19	Epitaxial growth of large-grain-size ferromagnetic monolayer CrI <sub>3</sub> for valley Zeeman splitting enhancement. Nanoscale, 2021, 13, 2955-2962.	5.6	5
20	Iridium Doping Boosting the Electrochemical Performance of Lithium-Rich Cathodes for Li-Ion Batteries. ACS Applied Energy Materials, 2021, 4, 2489-2495.	5.1	17
21	Synergistic Additiveâ€Assisted Growth of 2D Ternary In <sub>2</sub> SnS <sub>4</sub> with Giant Gateâ€Tunable Polarizationâ€Sensitive Photoresponse. Small, 2021, 17, e2008078.	10.0	18
22	Proximity Enhanced Hydrogen Evolution Reactivity of Substitutional Doped Monolayer WS <sub>2</sub> . ACS Applied Materials & Interfaces, 2021, 13, 19406-19413.	8.0	24
23	Ultrathin FeTe nanosheets with tetragonal and hexagonal phases synthesized by chemical vapor deposition. Materials Today, 2021, 45, 35-43.	14.2	29
24	Grain-boundary-rich polycrystalline monolayer WS2 film for attomolar-level Hg2+ sensors. Nature Communications, 2021, 12, 3870.	12.8	42
25	Twoâ€Ðimensionalâ€Germanium Phosphideâ€Reinforced Conductive and Biodegradable Hydrogel Scaffolds Enhance Spinal Cord Injury Repair. Advanced Functional Materials, 2021, 31, 2104440.	14.9	65
26	In Situ Phase Separation into Coupled Interfaces for Promoting CO <sub>2</sub> Electroreduction to Formate over a Wide Potential Window. Angewandte Chemie, 2021, 133, 23122-23129.	2.0	11
27	Photoemission oscillation in epitaxially grown van der Waals β-In <sub>2</sub> Se <sub>3</sub> WS <sub>2</sub> heterobilayer bubbles*. Chinese Physics B, 2021, 30, 117901.	1.4	0
28	In Situ Phase Separation into Coupled Interfaces for Promoting CO <sub>2</sub> Electroreduction to Formate over a Wide Potential Window. Angewandte Chemie - International Edition, 2021, 60, 22940-22947.	13.8	67
29	In Situ Grown Ultrafine RuO <sub>2</sub> Nanoparticles on GeP <sub>5</sub> Nanosheets as the Electrode Material for Flexible Planar Micro-Supercapacitors with High Specific Capacitance and Cyclability. ACS Applied Materials & Interfaces, 2021, 13, 47560-47571.	8.0	11
30	Origin of the improved reactivity of MoS2 single crystal by confining lattice Fe atom in peroxymonosulfate-based Fenton-like reaction. Applied Catalysis B: Environmental, 2021, 298, 120537.	20.2	53
31	High-sensitivity and versatile plasmonic biosensor based on grain boundaries in polycrystalline 1L WS2 films. Biosensors and Bioelectronics, 2021, 194, 113596.	10.1	13
32	Polypyrrole coated 3D flower MoS2 composites with tunable impedance for excellent microwave absorption performance. Journal of Alloys and Compounds, 2021, 888, 161487.	5.5	38
33	Atomic-Scale Visualization of Polar Domain Boundaries in Ferroelectric In <sub>2</sub> Se <sub>3</sub> at the Monolayer Limit. Journal of Physical Chemistry Letters, 2021, 12, 11902-11909.	4.6	7
34	Hierarchical iridium-based multimetallic alloy with double-core-shell architecture for efficient overall water splitting. Science China Materials, 2020, 63, 249-257.	6.3	59
35	Tailored architectures of FeNi alloy embedded in N-doped carbon as bifunctional oxygen electrocatalyst for rechargeable Zinc-air battery. Journal of Colloid and Interface Science, 2020, 561, 585-592.	9.4	59
36	All roads lead to Rome: Sodiation of different-stacked SnS2. Nano Energy, 2020, 67, 104276.	16.0	14

#	Article	IF	CITATIONS
37	Two-dimensional layered materials InSe nanoflakes/carbon nanotubes composite for flexible all-solid-state supercapacitors. Journal of Materials Science, 2020, 55, 2947-2957.	3.7	7
38	Direct one-step synthesis of CoFex@Co@C hybrids derived from a metal organic framework for a lightweight and high-performance microwave absorber. Nanotechnology, 2020, 31, 095703.	2.6	4
39	Room-temperature electric field modulation of magnetization in a helimagnet. Journal Physics D: Applied Physics, 2020, 53, 025001.	2.8	5
40	Inclined Ultrathin Bi <sub>2</sub> O <sub>2</sub> Se Films: A Building Block for Functional van der Waals Heterostructures. ACS Nano, 2020, 14, 16803-16812.	14.6	45
41	Revealing nanoscale mineralization pathways of hydroxyapatite using in situ liquid cell transmission electron microscopy. Science Advances, 2020, 6, .	10.3	61
42	Mechanical Robustness Two-Dimensional Silicon Phosphide Flake Anodes for Lithium Ion Batteries. ACS Sustainable Chemistry and Engineering, 2020, 8, 17597-17605.	6.7	15
43	Blackâ€Phosphorusâ€Incorporated Hydrogel as a Conductive and Biodegradable Platform for Enhancement of the Neural Differentiation of Mesenchymal Stem Cells. Advanced Functional Materials, 2020, 30, 2000177.	14.9	100
44	Pressure Effect on Order–Disorder Ferroelectric Transition in a Hydrogen-Bonded Metal–Organic Framework. Journal of Physical Chemistry Letters, 2020, 11, 9566-9571.	4.6	11
45	Direct observation of the formation and stabilization of metallic nanoparticles on carbon supports. Nature Communications, 2020, 11, 6373.	12.8	65
46	Honeycomb RhI <sub>3</sub> Flakes with High Environmental Stability for Optoelectronics. Advanced Materials, 2020, 32, e2001979.	21.0	27
47	Facile preparation of carbon nanosheet frameworks/magnetic nanohybrids with heterogeneous interface as an excellent microwave absorber. Journal of Alloys and Compounds, 2020, 838, 155586.	5.5	14
48	Application of hard ceramic materials B4C in energy storage: Design B4C@C core-shell nanoparticles as electrodes for flexible all-solid-state micro-supercapacitors with ultrahigh cyclability. Nano Energy, 2020, 75, 104947.	16.0	47
49	Orthogonal Electric Control of the Outâ€Ofâ€Plane Fieldâ€Effect in 2D Ferroelectric αâ€In <sub>2</sub> Se <sub>3</sub> . Advanced Electronic Materials, 2020, 6, 2000061.	5.1	56
50	Conversion of Intercalated MoO <sub>3</sub> to Multiâ€Heteroatomsâ€Doped MoS <sub>2</sub> with High Hydrogen Evolution Activity. Advanced Materials, 2020, 32, e2001167.	21.0	82
51	Direct Observation of Room-Temperature Dislocation Plasticity in Diamond. Matter, 2020, 2, 1222-1232.	10.0	48
52	Narrowing Working Voltage Window to Improve Layered GeP Anode Cycling Performance for Lithium-Ion Batteries. ACS Applied Materials & Interfaces, 2020, 12, 17466-17473.	8.0	33
53	Electric field control of nonvolatile twoâ€state magnetoelectric coefficient at room temperature in a hexaferrite. Journal of the American Ceramic Society, 2020, 103, 4384-4389.	3.8	6
54	Hydrogen Bond Tuning of Magnetoelectric Coupling in Metal–Organic Frameworks. Journal of Physical Chemistry C, 2020, 124, 16111-16115.	3.1	5

#	Article	IF	CITATIONS
55	Atomic-scale observation of the deformation and failure of diamonds by in-situ double-tilt mechanical testing transmission electron microscope holder. Science China Materials, 2020, 63, 2335-2343.	6.3	8
56	Photodetection application of one-step synthesized wafer-scale monolayer MoS2 by chemical vapor deposition. 2D Materials, 2020, 7, 025020.	4.4	13
57	Facile preparation of CoS2 nanoparticles embedded into polyaniline with tunable electromagnetic wave absorption performance. Materials Chemistry and Physics, 2020, 246, 122835.	4.0	31
58	Enhanced microwave absorption properties of MnS2 microspheres interspersed with carbon nanotubes. Journal of Magnetism and Magnetic Materials, 2020, 502, 166432.	2.3	13
59	Insight into Si poisoning on grain refinement of Al-Si/Al-5Ti-B system. Acta Materialia, 2020, 187, 51-65.	7.9	195
60	Atomically dispersed hierarchically ordered porous Fe–N–C electrocatalyst for high performance electrocatalytic oxygen reduction in Zn-Air battery. Nano Energy, 2020, 71, 104547.	16.0	206
61	Influence of van der Waals epitaxy on phase transformation behaviors in 2D heterostructure. Applied Physics Letters, 2020, 116, .	3.3	7
62	2D Hybrid Superlattice-Based On-Chip Electrocatalytic Microdevice for <i>in Situ</i> Revealing Enhanced Catalytic Activity. ACS Nano, 2020, 14, 1635-1644.	14.6	36
63	Highâ€Performance Broadband Photodetectors of Heterogeneous 2D Inorganic Molecular Sb <sub>2</sub> O <sub>3</sub> /Monolayer MoS <sub>2</sub> Crystals Grown via Chemical Vapor Deposition. Advanced Optical Materials, 2020, 8, 2000168.	7.3	17
64	Alloy engineered germanium monochalcogenide with tunable bandgap for broadband optoelectrical applications. Physical Review Materials, 2020, 4, .	2.4	5
65	Carbonaceous photonic crystals prepared by high-temperature/hydrothermal carbonization as high-performance microwave absorbers. Journal of Materials Science, 2019, 54, 14343-14353.	3.7	6
66	Layered porous materials indium triphosphide InP3 for high-performance flexible all-solid-state supercapacitors. Journal of Power Sources, 2019, 438, 227010.	7.8	17
67	Lateral Bilayer MoS <sub>2</sub> –WS <sub>2</sub> Heterostructure Photodetectors with High Responsivity and Detectivity. Advanced Optical Materials, 2019, 7, 1900815.	7.3	65
68	Submillimeter and lead-free Cs <sub>3</sub> Sb <sub>2</sub> Br <sub>9</sub> perovskite nanoflakes: inverse temperature crystallization growth and application for ultrasensitive photodetectors. Nanoscale Horizons, 2019, 4, 1372-1379.	8.0	85
69	Microwave absorption properties of heterostructure composites of two dimensional layered magnetic materials and graphene nanosheets. Applied Physics Letters, 2019, 115, .	3.3	23
70	Simple preparation and excellent microwave attenuation property of Fe3O4- and FeS2- decorated graphene nanosheets by liquid-phase exfoliation. Journal of Alloys and Compounds, 2019, 810, 151881.	5.5	13
71	Quasi-Two-Dimensional Se-Terminated Bismuth Oxychalcogenide (Bi <sub>2</sub> O <sub>2</sub> Se). ACS Nano, 2019, 13, 13439-13444.	14.6	61
72	One-step growth of wafer-scale monolayer tungsten disulfide via hydrogen sulfide assisted chemical vapor deposition. Applied Physics Letters, 2019, 115, .	3.3	13

#	Article	IF	CITATIONS
73	Coral-like Ni <sub>x</sub> Co <sub>1â^'x</sub> Se <sub>2</sub> for Na-ion battery with ultralong cycle life and ultrahigh rate capability. Journal of Materials Chemistry A, 2019, 7, 3933-3940.	10.3	85
74	Photoluminescence and Raman Spectra Oscillations Induced by Laser Interference in Annealingâ€Created Monolayer WS <sub>2</sub> Bubbles. Advanced Optical Materials, 2019, 7, 1801373.	7.3	21
75	Effect of layer and stacking sequence in simultaneously grown 2H and 3R WS <sub>2</sub> atomic layers. Nanotechnology, 2019, 30, 345203.	2.6	16
76	Atomic-Scale Observation of Reversible Thermally Driven Phase Transformation in 2D In <sub>2</sub> Se <sub>3</sub> . ACS Nano, 2019, 13, 8004-8011.	14.6	57
77	Enhanced cycling stability of high voltage LiCoO2 by surface phosphorylation. Journal of Alloys and Compounds, 2019, 803, 348-353.	5.5	21
78	Sodium storage mechanism and electrochemical performance of layered GeP as anode for sodium ion batteries. Journal of Power Sources, 2019, 433, 126682.	7.8	46
79	Highâ€Lithiumâ€Affinity Chemically Exfoliated 2D Covalent Organic Frameworks. Advanced Materials, 2019, 31, e1901640.	21.0	217
80	One-Step Growth of Spatially Graded Mo <sub>1–<i>x</i></sub> W <sub><i>x</i></sub> S <sub>2</sub> Monolayers with a Wide Span in Composition (from <i>x</i> = 0 to 1) at a Large Scale. ACS Applied Materials & Interfaces, 2019, 11, 20979-20986.	8.0	12
81	Ferroelectrics: Nonvolatile Ferroelectric Memory Effect in Ultrathin α″n 2 Se 3 (Adv. Funct. Mater.) Tj ETQq1 1	0.784314	4 rgβT /Over
82	<i>In situ</i> TEM and half cell investigation of sodium storage in hexagonal FeSe nanoparticles. Chemical Communications, 2019, 55, 5611-5614.	4.1	27
83	Accelerated Degradation of CrCl <sub>3</sub> Nanoflakes Induced by Metal Electrodes: Implications for Remediation in Nanodevice Fabrication. ACS Applied Nano Materials, 2019, 2, 1597-1603.	5.0	9
84	Small onion-like BN leads to ultrafine-twinned cubic BN. Science China Materials, 2019, 62, 1169-1176.	6.3	15
85	Uniform Lithium Deposition Assisted by Singleâ€Atom Doping toward Highâ€Performance Lithium Metal Anodes. Advanced Energy Materials, 2019, 9, 1804019.	19.5	151
86	Real-Time TEM Study of Nanopore Evolution in Battery Materials and Their Suppression for Enhanced Cycling Performance. Nano Letters, 2019, 19, 3074-3082.	9.1	29
87	Nonvolatile Ferroelectric Memory Effect in Ultrathin αâ€In <sub>2</sub> Se <sub>3</sub> . Advanced Functional Materials, 2019, 29, 1808606.	14.9	137
88	Atomically Resolving Polymorphs and Crystal Structures of In <sub>2</sub> Se <sub>3</sub> . Chemistry of Materials, 2019, 31, 10143-10149.	6.7	71
89	Approaching diamond's theoretical elasticity and strength limits. Nature Communications, 2019, 10, 5533.	12.8	73
90	Static and dynamic characteristics of magnetism in permalloy oval nanoring by micromagnetic simulation. Journal of Magnetism and Magnetic Materials, 2019, 474, 301-304.	2.3	15

#	Article	IF	CITATIONS
91	Microwave absorbing properties of two dimensional materials GeP5 enhanced after annealing treatment. Applied Physics Letters, 2019, 114, .	3.3	24
92	Liquid-exfoliation of S-doped black phosphorus nanosheets for enhanced oxygen evolution catalysis. Nanotechnology, 2019, 30, 035701.	2.6	32
93	A numerical study on striped lithiation of tin oxide anodes. International Journal of Solids and Structures, 2019, 159, 163-170.	2.7	2
94	Characterization of Nanomaterials by Electron Microscopy. World Scientific Series in Nanoscience and Nanotechnology, 2019, , 35-173.	0.1	0
95	Grain wall boundaries in centimeter-scale continuous monolayer WS <sub>2</sub> film grown by chemical vapor deposition. Nanotechnology, 2018, 29, 255705.	2.6	14
96	Nanoceria-Supported Single-Atom Platinum Catalysts for Direct Methane Conversion. ACS Catalysis, 2018, 8, 4044-4048.	11.2	214
97	Carbothermal shock synthesis of high-entropy-alloy nanoparticles. Science, 2018, 359, 1489-1494.	12.6	1,065
98	Scanning distortion correction in STEM images. Ultramicroscopy, 2018, 184, 274-283.	1.9	23
99	In Situ Transmission Electron Microscopy Explores a New Nanoscale Pathway for Direct Gypsum Formation in Aqueous Solution. ACS Applied Nano Materials, 2018, 1, 5430-5440.	5.0	22
100	Cracks Formation in Lithium-Rich Cathode Materials for Lithium-Ion Batteries during the Electrochemical Process. Energies, 2018, 11, 2712.	3.1	7
101	Facile Synthesis of Carbon-Encapsulated Ni Nanoparticles Embedded into Porous Graphite Sheets as High-Performance Microwave Absorber. ACS Sustainable Chemistry and Engineering, 2018, 6, 16179-16185.	6.7	15
102	Systematic investigation of the Binder's role in the electrochemical performance of tin sulfide electrodes in SIBs. Journal of Power Sources, 2018, 401, 195-203.	7.8	23
103	Metallic layered germanium phosphide GeP <sub>5</sub> for high rate flexible all-solid-state supercapacitors. Journal of Materials Chemistry A, 2018, 6, 19409-19416.	10.3	31
104	Highâ€Temperature Atomic Mixing toward Wellâ€Dispersed Bimetallic Electrocatalysts. Advanced Energy Materials, 2018, 8, 1800466.	19.5	43
105	Metal–organic framework derived cobalt phosphosulfide with ultrahigh microwave absorption properties. Nanotechnology, 2018, 29, 405703.	2.6	30
106	Improved Electrochemical Performances of LiCoO <sub>2</sub> at Elevated Voltage and Temperature with an In Situ Formed Spinel Coating Layer. ACS Applied Materials & Interfaces, 2018, 10, 31271-31279.	8.0	81
107	In Situ, Fast, Highâ€Temperature Synthesis of Nickel Nanoparticles in Reduced Graphene Oxide Matrix. Advanced Energy Materials, 2017, 7, 1601783.	19.5	27
108	Sodium-Induced Reordering of Atomic Stacks in Black Phosphorus. Chemistry of Materials, 2017, 29, 1350-1356.	6.7	55

#	Article	IF	CITATIONS
109	A Strategy for Synthesis of Nanosheets Consisting of Alternating Spinel Li <sub>4</sub> Ti <sub>5</sub> O <sub>12</sub> and Rutile TiO <sub>2</sub> Lamellas for High-Rate Anodes of Lithium-Ion Batteries. ACS Applied Materials & Interfaces, 2017, 9, 4649-4657.	8.0	42
110	Facet-Dependent Thermal Instability in LiCoO <sub>2</sub> . Nano Letters, 2017, 17, 2165-2171.	9.1	99
111	<i>In Situ</i> High Temperature Synthesis of Single-Component Metallic Nanoparticles. ACS Central Science, 2017, 3, 294-301.	11.3	34
112	Lithium metal protected by atomic layer deposition metal oxide for high performance anodes. Journal of Materials Chemistry A, 2017, 5, 12297-12309.	10.3	150
113	Direct evidence of M2 phase during the monoclinic-tetragonal (rutile) phase transition of W-doped VO2 nanowires. Applied Physics Letters, 2017, 110, .	3.3	11
114	Discovering a First-Order Phase Transition in the Li–CeO <sub>2</sub> System. Nano Letters, 2017, 17, 1282-1288.	9.1	27
115	Strain Release Induced Novel Fluorescence Variation in CVD-Grown Monolayer WS <sub>2</sub> Crystals. ACS Applied Materials & Interfaces, 2017, 9, 34071-34077.	8.0	17
116	In Situ TEM Investigation of ZnO Nanowires during Sodiation and Lithiation Cycling. Small Methods, 2017, 1, 1700202.	8.6	45
117	In situ cooling and heating study of VO 2 phase transition. Microscopy and Microanalysis, 2016, 22, 816-817.	0.4	0
118	Atomic Resolution Studies of W Dopants Effect on the Phase Transformation of VO2. Microscopy and Microanalysis, 2016, 22, 884-885.	0.4	1
119	Atomistic Exploration of the Surface-Sensitive Oriented Attachment Growth of a-MnCh Nanowires and the Formation of Defective Interface with 2Å—3 and 2Å—4 Tunnel Intergrowth. Microscopy and Microanalysis, 2016, 22, 386-387.	0.4	0
120	Effect of Mechanical Stress on Lithiation and Sodiation Process. Microscopy and Microanalysis, 2016, 22, 1382-1383.	0.4	0
121	Transmission Electron Microscopy Studies of Calcium Phosphate Biomineralization. Microscopy and Microanalysis, 2016, 22, 798-799.	0.4	0
122	In-situ TEM Investigation on Thermal Stability and Oxygen Release Behavior of Charged and Discharged LiCoO2. Microscopy and Microanalysis, 2016, 22, 844-845.	0.4	0
123	<i>In Situ</i> Transmission Electron Microscopy Observation of Sodiation–Desodiation in a Long Cycle, High-Capacity Reduced Graphene Oxide Sodium-Ion Battery Anode. Chemistry of Materials, 2016, 28, 6528-6535.	6.7	79
124	The influence of large cations on the electrochemical properties of tunnel-structured metal oxides. Nature Communications, 2016, 7, 13374.	12.8	180
125	Ultrafast and Highly Reversible Sodium Storage in Zincâ€Antimony Intermetallic Nanomaterials. Advanced Functional Materials, 2016, 26, 543-552.	14.9	81
126	Dynamic study of (De)sodiation in alpha-MnO2 nanowires. Nano Energy, 2016, 19, 382-390.	16.0	54

#	Article	IF	CITATIONS
127	Selective Ionic Transport Pathways in Phosphorene. Nano Letters, 2016, 16, 2240-2247.	9.1	79
128	Atomistic Insights into the Oriented Attachment of Tunnel-Based Oxide Nanostructures. ACS Nano, 2016, 10, 539-548.	14.6	66
129	In situ TEM Observation of Lithiation and Sodiation Process of ZnO Nanowire. Microscopy and Microanalysis, 2015, 21, 1371-1372.	0.4	2
130	In Situ TEM Characterization of Nanostructured Dielectrics. Microscopy and Microanalysis, 2015, 21, 1813-1814.	0.4	1
131	Can Na+ Transport Faster Than Li+ inside Zn-Sb Intermetallic Nanomaterials?. Microscopy and Microanalysis, 2015, 21, 1195-1196.	0.4	2
132	Dynamic Study of Sodiation Process in Single Crystalline a-MnO2 Nanowires. Microscopy and Microanalysis, 2015, 21, 1543-1544.	0.4	0
133	Capacity retention behavior and morphology evolution of Si <i><sub>x</sub></i> Ge <sub>1â^'<i>x</i></sub> nanoparticles as lithium-ion battery anode. Nanotechnology, 2015, 26, 255702.	2.6	13
134	Atomic resolution observation of conversion-type anode RuO <sub>2</sub> during the first electrochemical lithiation. Nanotechnology, 2015, 26, 125404.	2.6	14
135	In situ study on stability of copper oxide nanomaterials by e-beam irradiation. Materials Letters, 2015, 156, 134-137.	2.6	3
136	Asynchronous Crystal Cell Expansion during Lithiation of K <sup>+</sup> -Stabilized α-MnO <sub>2</sub> . Nano Letters, 2015, 15, 2998-3007.	9.1	161
137	Atomic Origins of Monoclinic-Tetragonal (Rutile) Phase Transition in Doped VO <sub>2</sub> Nanowires. Nano Letters, 2015, 15, 7179-7188.	9.1	52
138	A global view of the phase transitions of SnO <sub>2</sub> in rechargeable batteries based on results of high throughput calculations. Journal of Materials Chemistry A, 2015, 3, 19483-19489.	10.3	21
139	Twin Boundary-Assisted Lithium Ion Transport. Nano Letters, 2015, 15, 610-615.	9.1	80
140	Evolution of Lattice Structure and Chemical Composition of the Surface Reconstruction Layer in Li <sub>1.2</sub> Ni <sub>0.2</sub> Mn <sub>0.6</sub> O <sub>2</sub> Cathode Material for Lithium Ion Batteries. Nano Letters, 2015, 15, 514-522.	9.1	261
141	<i>In Situ</i> Study of Thermal Stability of Copper Oxide Nanowires at Anaerobic Environment. Journal of Nanomaterials, 2014, 2014, 1-6.	2.7	7
142	Insight into Sulfur Reactions in Li–S Batteries. ACS Applied Materials & Interfaces, 2014, 6, 21938-21945.	8.0	120
143	Direct Evidence of Lithium-Induced Atomic Ordering in Amorphous TiO <sub>2</sub> Nanotubes. Chemistry of Materials, 2014, 26, 1660-1669.	6.7	75
144	Origin of the Phase Transition in Lithiated Molybdenum Disulfide. ACS Nano, 2014, 8, 11447-11453.	14.6	111

#	Article	IF	CITATIONS
145	Lithiation-Induced Shuffling of Atomic Stacks. Nano Letters, 2014, 14, 5301-5307.	9.1	18
146	<i>In situ</i> high resolution transmission electron microscopy investigation of deformation mechanism in sub-10-nm Au crystals. Materials Science and Technology, 2014, 30, 774-781.	1.6	6
147	Direct Atomic-Scale Imaging of Multistep Phase Transition during the Lithiation of Nanowires by In-Situ (S)TEM. Microscopy and Microanalysis, 2014, 20, 428-429.	0.4	0
148	In-situ TEM Study on Electrochemical Behavior of α-MnO <sub>2</sub> Nanowire. Microscopy and Microanalysis, 2014, 20, 496-497.	0.4	2
149	Atomic Resolution Study of Local Strains in Doped VO2 Nanowires. Microscopy and Microanalysis, 2014, 20, 1074-1075.	0.4	0
150	Atomic-Scale Observation of Lithiation Reaction Front in Nanoscale SnO <sub>2</sub> Materials. ACS Nano, 2013, 7, 6203-6211.	14.6	134
151	Structural and Electrochemical Study of Al <sub>2</sub> O <sub>3</sub> and TiO <sub>2</sub> Coated Li <sub>1.2</sub> Ni <sub>0.13</sub> Mn <sub>0.54</sub> Co <sub>0.13</sub> O <sub>2</sub> Cathode Material Using ALD. Advanced Energy Materials, 2013, 3, 1299-1307.	19.5	418
152	Microstructure-Dependent Conformal Atomic Layer Deposition on 3D Nanotopography. Langmuir, 2012, 28, 15809-15815.	3.5	6
153	Epitaxial TiO2/SnO2 core–shell heterostructure by atomic layer deposition. Journal of Materials Chemistry, 2012, 22, 10665.	6.7	34
154	Nanofingers pulled from bulk silver. Scripta Materialia, 2012, 66, 247-249.	5.2	1
155	Catalytic Oxidation of Chlorobenzene over V <sub>2</sub> O <sub>5</sub> /TiO <sub>2</sub> –Carbon Nanotubes Composites. Industrial & Engineering Chemistry Research, 2011, 50, 9944-9948.	3.7	45
156	Electrical failure behaviors of semiconductor oxide nanowires. Nanotechnology, 2011, 22, 405703.	2.6	19
157	Molecular dynamics simulation on deformation mechanisms in body-centered-cubic molybdenum nanowires. Journal of Applied Physics, 2011, 110, .	2.5	52
158	In situ TEM study on crack propagation in nanoscale Au thin films. Scripta Materialia, 2011, 65, 377-379.	5.2	30
159	Grain boundary structure dependent fracture in nanocrystalline Au films. Materials Letters, 2011, 65, 2769-2771.	2.6	10
160	Deformation-mediated phase transformation in gold nano-junction. Materials Letters, 2011, 65, 3380-3383.	2.6	18
161	Catalytic Oxidation of Chlorobenzene over MnO x /Al2O3-carbon Nanotubes Composites. Catalysis Letters, 2011, 141, 158-162.	2.6	31
162	Catalytic Reduction of NO with NH3 over V2O5-MnOX/TiO2-Carbon Nanotube Composites. Catalysis Letters, 2011, 141, 1237-1242.	2.6	34

#	Article	IF	CITATIONS
163	Defect-driven room-temperature coalescence of double-walled carbon nanotubes. Nanotechnology, 2010, 21, 245302.	2.6	8
164	Oxygen Impurity in Cubic Boron Nitride Thin Films Prepared by Plasma-enhanced Chemical Vapor Deposition. Wuji Cailiao Xuebao/Journal of Inorganic Materials, 2010, 25, 748-752.	1.3	2